

EXPERIMENTAL STUDY OF BATHYMETRY VARIATION EFFECTS ON A CROSS-FLOW WATER TURBINE

Noam Bloch⁽¹⁾, Martin Moreau^(1,2), Grégory Germain⁽¹⁾, Guillaume Maurice⁽²⁾
noam.bloch@ifremer.fr ; martin.moreau@ifremer.fr (corresponding author)
gregory.germain@ifremer.fr ; guillaume.maurice@hydroquest.net

⁽¹⁾Ifremer, Marine Hydrodynamic Laboratory, Boulogne-sur-Mer, France

⁽²⁾HydroQuest SAS, Meylan, France

Résumé

D'importants détachements tourbillonnaires sont générés dans le sillage de variations bathymétriques rencontrées dans les sites hydroliens. Dans ce travail, nous étudions expérimentalement l'impact de ces structures sur le comportement d'une hydrolienne carénée à double axe vertical à double rotors contrarotatifs. Dans ce but, un modèle à l'échelle 1/20^{ème} du démonstrateur de 1MW développé par HydroQuest a été placé dans le sillage de différents obstacles posés au fond du bassin à houle et courant de l'Ifremer. Dans ces conditions, l'hydrolienne est soumise à l'impact régulier de structures tourbillonnaires émises dans le sillage de l'obstacle. Les résultats montrent que les valeurs moyennes des coefficients de puissance et de traînée appliqués sur l'hydrolienne diminuent dans le sillage des obstacles du fait du ralentissement de l'écoulement (respectivement de 41 et 25%). Les fluctuations de ces quantités augmentent quant à elles significativement quelle que soit la position considérée (respectivement d'un facteur 2.8 et 1.8). Ces effets doivent donc être pris en compte pour le dimensionnement des machines.

Summary

Significant vortex shedding are generated in the wake of bathymetric variations encountered in tidal energy sites. In this work, we experimentally study the impact of these energetic structures on the behaviour of a ducted twin counter-rotating vertical axis turbine. To this end, a 1/20 scale model of the 1MW rated demonstrator developed by HydroQuest is placed in the wake of various obstacles on the bottom of Ifremer's wave and current flume tank. Under these conditions, the tidal turbine is subjected to the regular impact of vortex structures emitted in the wake of the obstacle. The results show that the mean value of the power and drag coefficients applied to the tidal turbine decrease in the wake of the obstacles due to the slowing down of the flow (respectively by 41 and 25%). The fluctuations of these quantities increase significantly regardless of the position considered (respectively by a factor of 2.8 and 1.8). These effects must therefore be taken into account for the turbine design.

I – Introduction

Considering the climate change that we are now facing and the ever growing energy demand, renewable energy technologies show an important growth. Solar and wind are headlining the market but tidal energy converters (TEC) are making their way too. In Europe, the most energetic spots are mainly located in France and the United Kingdom [6]. *HydroQuest* is one of the companies in line to implement full-scale TECs after more than ten years of design and development. Its concept is composed of two counter-rotating vertical axis energy converters installed on a gravity base. Between 2019 and 2021, a 1 MW rated demonstrator was tested at EDF’s test site in Paimpol-Bréhat, France [12]. This step provided the company an important insight on the turbine’s behaviour at full-scale. For further developments of its twin vertical axis tidal turbine (2-VATT), to isolate design parameters and save both money and time, the company wishes to better rely on lab-scale experiments. This can only be achieved by comparing the experimental results to those obtained at sea. To that aim, a lab-scale model, similar to the demonstrator, was designed with a scale factor $\epsilon = 1/20$. This model has been tested in several conditions in the Ifremer’s wave and current flume tank, located in Boulogne-sur-Mer, France [13].

Experiments conducted in Ramsey Sound (Wales, United Kingdom) show on another kind of tidal turbine the necessity to know the bathymetry for accurate performance assessment, as a reduced inflow and an increased turbulence may lower the turbine’s performance compared to numerical predictions [7]. Indeed, it has been shown that a high level of turbulence can have a significant effect on a TEC’s behaviour, decreasing slightly the mean values of its performance while increasing substantially their fluctuations [2, 15]. Experimental studies conducted on an horizontal axis tidal turbine (HATT) indicates that bathymetry variations generate important turbulent structures which can impact the TEC, inducing intense and periodic load fluctuations [5]. The aforementioned HATT experiences a local flow velocity varying with the type of bathymetry encountered and the distance between the turbine and the bathymetry variations [10]. This phenomenon needs to be taken into account as the evaluation of the incident flow velocity plays an important role in the turbine’s performance assessment. However, the HATT studied in [5, 10] and the present 2-VATT have different geometries and flow direction sensitivity. Their location in the water column is also different. They are hence likely to be impacted differently by bathymetry variations.

The present work focuses on assessing experimentally the impact of bathymetry variations on the bottom-mounted 2-VATT from the comparison of two bathymetric configurations with an ideal flat floor. The turbine model and the experimental set-up is first described in section II. Section III presents the effects of bathymetry variations on the global turbine behaviour (III.1) with an analysis on both the temporal (III.2) and spectral domain (III.3). Finally, we discuss and conclude the results in Section IV.

II – Materials and Methods

II – 1 Turbine model

The 2-VATT model is geometrically similar to *HydroQuest*’s demonstrator at a 1/20 scale [13]. It is composed of two independent counter-rotating vertical axis rotor columns. Each column is made of two levels of rotors with a 60° phase difference between them, and each rotor is made of three blades with NACA 0018 profiles projected on the swept cylinder. The rotors radius ($R = D/2$) is 200 mm with blades chord of 73 mm and a blade height (H_{blade}) equal to 190 mm. The columns are mounted in a $W_{model} = 1.24$ m wide mechanical structure made of fairings and plates. The overall model height, from the floor to the top of the structure is $H_{model} = 840$ mm. The turbine height is defined as the distance between the top and the bottom horizontal plates such that $H = 450$ mm.

The central fairing of the turbine and the volume inside the top casing are watertight to host the electronic and the transmission system (Fig. 1). Indeed, the rotor shafts are linked to

secondary shafts (one by rotor column) through a belt system on the top of the turbine. Each secondary column is composed of a *Maxon RE50* DC motor equipped with a $1/26^{th}$ gear reducer and a speed encoder. A *Scaime DR2112-W* torque-meter with a relative angular position encoder also composes the column. The motors are piloted using remote *Escon 70/10* servo-controllers in constant speed mode. In addition, the turbine is fixed on a tripod base through a 6-component load cells (*SIXAXES* 1.5 kN) in order to model the demonstrator’s gravity base. At lab-scale, the model is fixed to the tank floor at the bottom of the central pile of the base, right below the turbine, on another 6-component load cell (*SIXAXES* 20 kN) to measure the overall loads on the turbine and the base. The tripod piles are 1 cm above the floor to avoid interference with the load cell measurements.

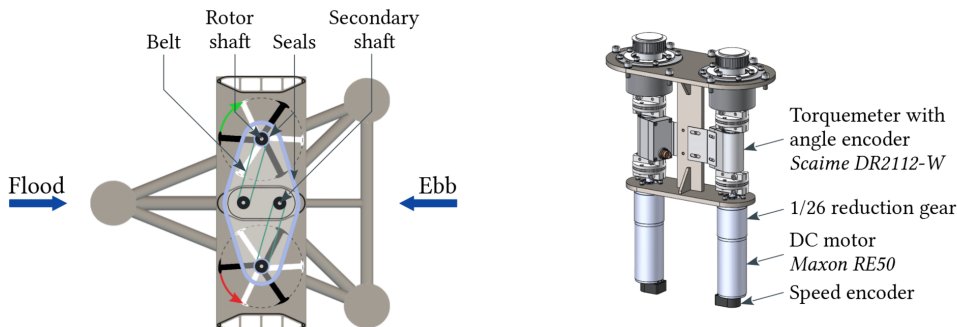


FIGURE 1 – Schematic top view of the twin counter-rotating VATT model (on the left) and the instrumentation, located in the central part of the model (on the right).

II – 2 Ifremer flume tank

The 2-VATT model is tested in the Ifremer wave and current flume tank in Boulogne-sur-mer, France (Fig. 2). The test section is $H_{tank} = 2$ m deep and $W_{tank} = 4$ m wide with a working section of approximately 18 m long [4]. Thus, the vertical blockage in the tank (H_{model}/H_{tank}) is equal to the one in-situ (41 %). Consequently, the projected surface blockage ($b = \frac{(HW)_{model}}{(HW)_{tank}}$), is about 12 % in the tank with the base, and 8 % with the turbine only. According to the literature review in [14], this surface blockage ratio is on the edge between small enough and too high values to consider results as they are. Corrections due to some blockage effects might be needed to estimate power performance accurately, like done in [1].

The orthogonal coordinates system considered is such that the streamwise coordinate x is in the current direction and the spanwise coordinate y is oriented from the observation window towards the wall. Both origins are set at the centre of the model. Finally, z points towards the surface with its origin on the tank floor. The three instantaneous velocity components are noted (U, V, W) along the (x, y, z) directions respectively. Using the Reynolds decomposition, each instantaneous velocity component is separated into a mean value and a fluctuating part : $U = \bar{U} + u'$, where the overbar indicates the time average. In the following, the average Reynolds shear stress corresponds to $\tau_{uw} = \overline{u'w'}$.

The inlet condition in the tank is conditioned by a homogeneous grid and a honeycomb structure. The streamwise turbulent intensity is defined as $TI_u = \sigma(U)/\bar{U}$, where σ is the standard deviation. Considering the empty tank, it appears that the boundary layer extends up to the bottom of the turbine, with TI_u decreasing from 7.5 to 1.5 % [13]. The turbulent intensity and streamwise velocity profiles are then uniform over the turbine height. The tests are conducted at a current set point of 1 m.s^{-1} . This is similar to a full-scale velocity of 4.5 m.s^{-1} according to Froude similitude law, which is in the range of tidal current velocities present at sea in areas suitable for tidal applications [3]. At this speed, the Reynolds number based on the blade chord and the rotational speed is of the order of 10^5 in the tank, which is about 100 times lower than the Reynolds number at full scale.

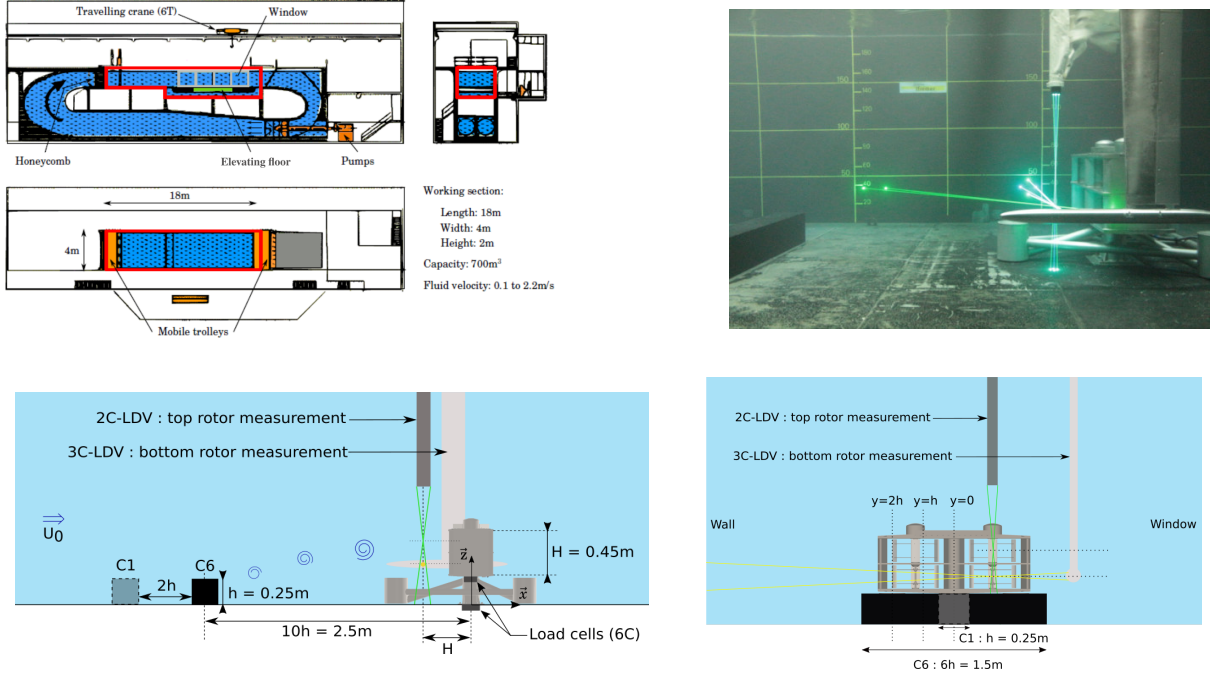


FIGURE 2 – Top : schematic view of the Ifremer’s flume tank and illustration of LDV measurement. Bottom : Schematic view of the experimental set-up

II – 3 Bottom-mounted obstacles

Previous studies lead in the Ifremer flume tank showed that the main flow characteristics induced by bathymetry variations in-situ could be modelled using simple bottom-mounted obstacles [8, 9, 10, 11]. The obstacles chosen in the present work are a square cylinder and a cube, both square sections side being of dimension $h = 0.25$ m. The length of the cylinder is $6h$, corresponding to an aspect ratio of 6. Two configurations are then studied : the cylinder isolated (C6) and a tandem configuration where the cube is placed $2h$ upstream of the cylinder (C1C6). Ikhennicheu et al. [8] showed that isolated obstacles with a large aspect ratio, like C6, produce the most energetic wakes with vortices rising up to the free surface. However, when a cube is placed ahead of the cylinder, like for C1C6, the wake development is deeply modified. The present work analyses the differences for the turbine operation when it is placed behind those obstacles.

Fig. 3 and 4 recall the wake generated by the obstacles without turbine, both in terms of streamwise velocity and shear stress, as presented in [10]. Those wake maps are made along three planes following the y -direction : at $y = 0$, $y = h$ and $y = 2h$. The symmetry is assumed for the y -negative part of the tank. The general pattern for the mean velocity in the C6 wake is a flow detachment at the leading edge of the cylinder, resulting in a recirculation zone and an outer steady region, separated by a shear layer with a strong velocity gradient. The flow reattaches further downstream. While the wake of C1C6 looks similar to C6 at $y = 2h$, the presence of the cube deeply modifies the flow behaviour when we look closer to the symmetry plane. There, the cube wake hits the cylinder and therefore modifies the global wake development : the recirculation area is smaller for C1C6 than for C6 and the shear layer reaches an upper limit of approximately $z = 3.5h$ behind C1C6 whereas its height keeps increasing behind C6.

The average Reynolds shear stress (Fig. 4) is a good marker of the shear layer and of the generated turbulence. Apart from the $y = 2h$ planes, where the shear stresses are very much alike, shear layers appear smaller and less intense for C1C6 than for C6. Moreover, spectral analyses conducted on the wake of those two configurations revealed the shedding of large energetic vortices at a frequency around 0.25 Hz [5, 9, 10, 11]. However, they behave differently depending on the configuration. Behind C6, the vortices form quickly downstream the obstacle and are ejected towards the free surface. On the other hand, behind C1C6, they are visible only further

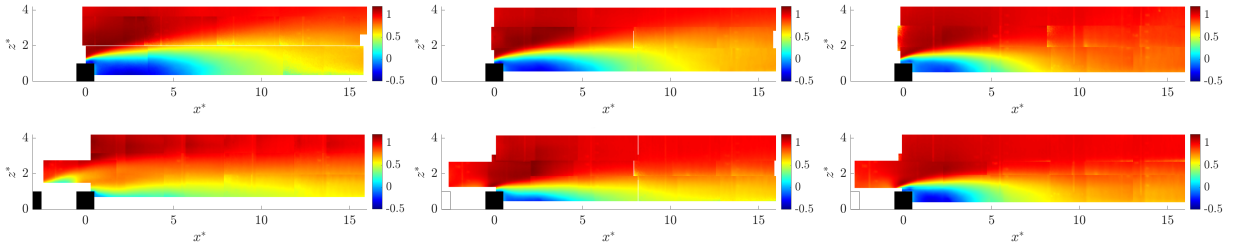


FIGURE 3 – Mean streamwise velocity \bar{U} behind C6 (top) and C1C6 (bottom) with $x^* = x/h$, $y^* = y/h$ and $z^* = z/h$. Left : $y^* = 0$; middle : $y^* = 1$; right : $y^* = 2$, [10].

in the wake as they need more time to aggregate. The vortices are also smaller than behind C6 and their movement is horizontal as they do not rise in the water column. The cube wake inhibits the development of the energetic and upward-directed wake of the cylinder.

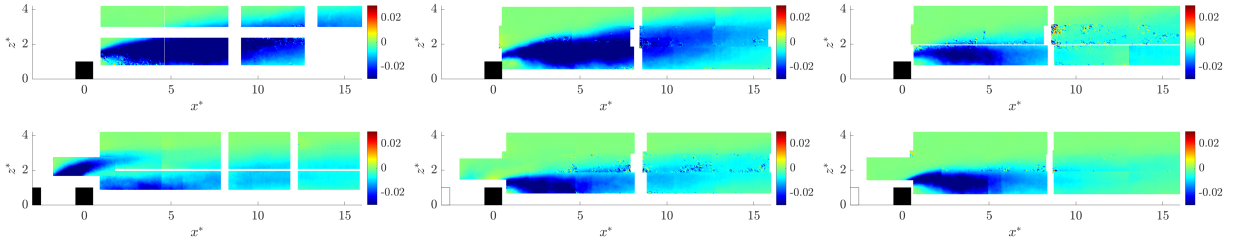


FIGURE 4 – Average Reynolds shear stress τ_{uw} behind C6 (top) and C1C6 (bottom) with $x^* = x/h$, $y^* = y/h$ and $z^* = z/h$. Left : $y^* = 0$; middle : $y^* = 1$; right : $y^* = 2$, [10].

Given the wake developments in the two configurations, both set of obstacles are placed upstream of the turbine, either at $x = -10h$ or $x = -16h$, and are compared with the denoted "Flat floor" case for which no obstacle is set in the tank.

II – 4 Data acquisition and processing

The torques (Q), the rotational speeds (ω), the angular positions of the two columns as well as the signals from the two load cells are acquired synchronously using *National Instruments PXI* and *LabView* systems. The acquisition frequency is set at 128 Hz during 3 minutes per run in the Flat floor case and 5 minutes per run with the obstacles to guarantee the time convergence of the mean and standard deviation of the signals. The performance results are presented in terms of power coefficient (C_P) and drag coefficient (C_x) with regard to the tip speed ratio (λ), defined in Eq. 1; with ρ the water density, P the power extracted by the two columns ($P = \sum \omega Q$) and F_x the load in the streamwise direction measured by the upper load cell. The reference surface considered is the projected area of the four rotors ($4DH_{blade}$). The reference velocity, $U_0 = 0.944 \text{ m.s}^{-1}$, is the mean streamwise component of the velocity far ahead of the turbine measured during prior tests, on a flat floor, at the center of the turbine [13]. It is considered as the constant reference velocity to compute the hydrodynamic coefficients for all cases, either with or without bathymetry obstacle.

$$C_P = \frac{P}{2\rho DH_{blade} U_0^3} \quad C_x = \frac{F_x}{2\rho DH_{blade} U_0^2} \quad \lambda = \frac{\omega R}{U_0} \quad (1)$$

For fluid-structure interaction assessment, the current velocity is measured using two *Dantec* Laser Doppler Velocimeters (LDV). They are placed in the induction zone, at $x = -H$, facing the rotors axis, that is to say at $y = -0.31 \text{ m}$ (Fig. 2). The 2-Component LDV (2C-LDV) is put in front of the upper rotor ($z = 0.61 \text{ m}$) and the 3-Component one (3C-LDV) is in front of the lower rotor ($z = 0.41 \text{ m}$). They both measure the velocity components in non-coincident mode.

The 3C-LDV works similarly to the 2C-LDV (which measures U, V along x, y) but given the orientation of the three pairs of lasers, it is necessary to project the probe measurements into the tank coordinate system to get (U, V, W) along (x, y, z) . To do so, the measurements in the lasers coordinate system are interpolated on the same time vector to apply the transformation matrix. The acquisition data rate is of the order of 150 Hz for both probes.

III – Bathymetry variation effects on turbine behaviour

III – 1 Effects on the global performance

Fig. 5 presents scatter plots of the torque and the rotational speed of the rotors for every acquisition point during a run. Those data are at the operating point giving the best average power coefficient, which is not the same point for each configuration as shown in Fig. 6 (between $\lambda = 1.38$ and $\lambda = 1.59$). It appears that the presence of an obstacle in the flow generates huge fluctuations in the turbine’s operation. The dispersion is also slightly lower behind C1C6 than behind C6. It shows that the turbulence generated by the bathymetry has a substantial impact on the turbine which depends on the bathymetry configuration. Another noteworthy point is the fact that the torque is below 0 Nm part of the time in the cases with obstacles. At lab scale, the regulation keeps the rotational speed constant with a high gain. Therefore, the 2-VATT sometimes needs energy to stay at the set point and thus works in motor mode in the obstacles’ wake. It also leads to the noticeable cluster around 0 Nm which is explained by the recovery of mechanical plays when switching between generator and motor modes.

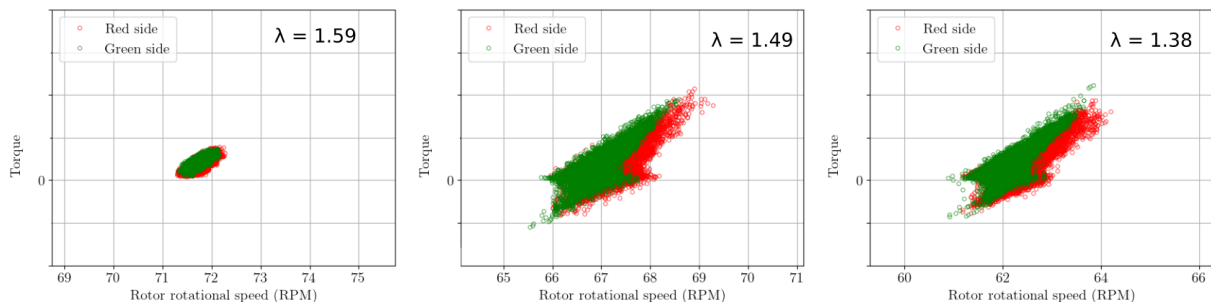


FIGURE 5 – Torque as a function of the rotor rotational speed at the best performance point. Left : Flat floor ; middle : C6 at $x = -16h$; right : C1C6 at $x = -16h$.

Fig. 6 displays the power and drag coefficients (Eq. 1), in terms of mean value and standard deviation, with respect to the tip speed ratio. Between C6 and Flat floor cases, \overline{Cp} decreases strongly behind the obstacle : at the optimum point, it plummets by 41 % with the cylinder at $x = -10h$ and by 33 % at $x = -16h$. Two factors are involved in this drop of \overline{Cp} . First, we use the same U_0 value for coefficients calculation in Flat floor and C6 while physically the flow velocity is reduced in the cylinder wake. Then, the turbulence is much higher behind the obstacle and [2] showed that an increase of turbulence reduces the power coefficient by up to 10 % in extreme cases. The standard deviation of Cp at the optimum point is multiplied by 2.4 at $x = -10h$ and by 2.0 at $x = -16h$ from Flat floor to C6. This must be due to the turbulence increase in the obstacle wake and to the periodic vortex shedding as shown on a HATT [5]. The same pattern applies for the drag, but with smaller differences. From Flat floor to C6, \overline{Cx} decreases by 23 % at $x = -10h$ and by 19 % at $x = -16h$ while its standard deviation is greater by a factor 1.8 at $x = -10h$ and 1.6 at $x = -16h$. The shift of the curves along the tip speed ratio axis is also due to the use of a reference velocity greater than the one perceived by the turbine. In C6, the cylinder’s impact is greater when the turbine is closer. This is consistent with the wake maps in Fig. 3. Indeed, the average velocity over the capture area of the turbine ($0.28 \text{ m} < z < 0.73 \text{ m}$) at $x = -10h$ is lower than at $x = -16h$ so there is no surprise we find $\overline{Cp}(x = -10h) < \overline{Cp}(x = -16h)$ and $\overline{Cx}(x = -10h) < \overline{Cx}(x = -16h)$. Furthermore,

Fig. 4 shows a greater level of turbulence at $x = -10h$ than at $x = -16h$, thereby leading to $\sigma(Cp(x = -10h)) > \sigma(Cp(x = -16h))$ and $\sigma(Cx(x = -10h)) > \sigma(Cx(x = -16h))$.

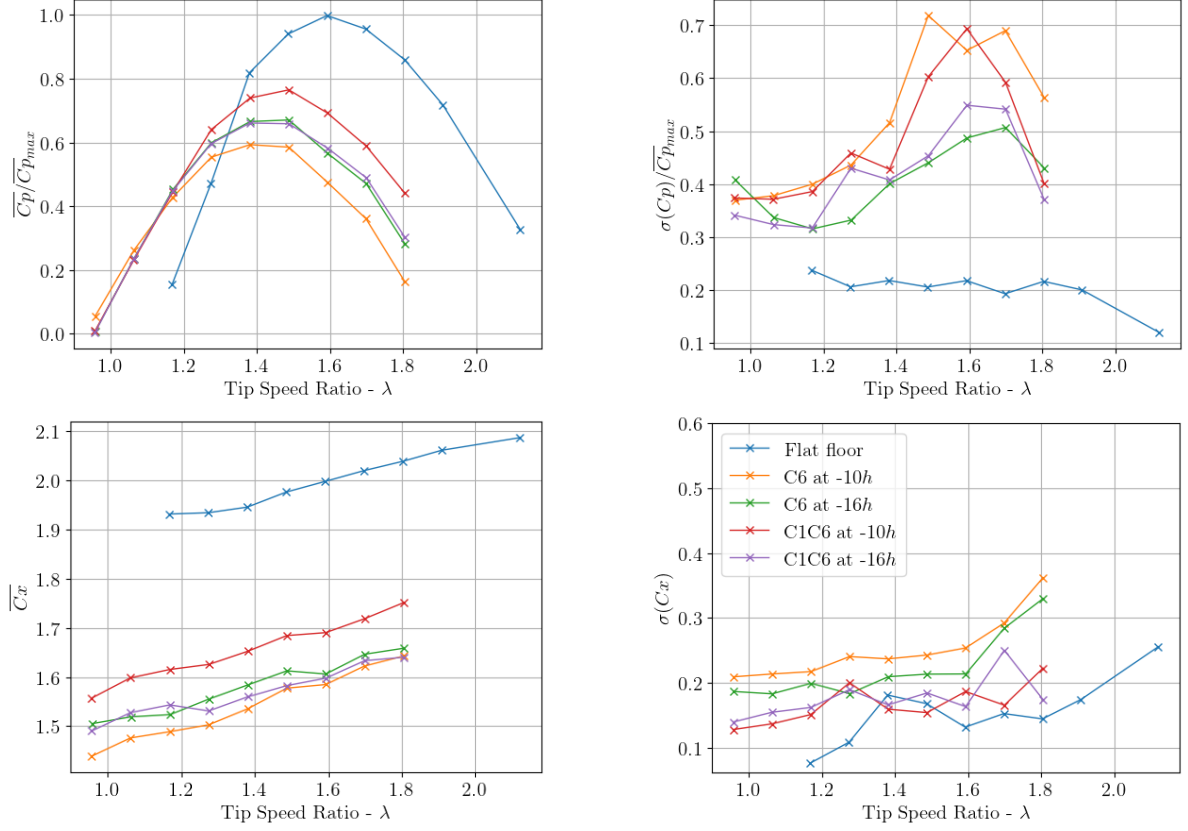


FIGURE 6 – Power (top) and drag (bottom) coefficients. Left : Mean value over a run; right : standard deviation

Looking at the C1C6 case curves, \overline{Cp} and \overline{Cx} also decrease behind the obstacle compared to the Flat floor case : at the optimum operating point, they drop respectively by 23 and 16 % at $x = -10h$ and by 34 and 22 % at $x = -16h$. However, the effect of the downstream distance is reversed from what it is behind C6 since \overline{Cp} and \overline{Cx} are lower far from the obstacles ($x = -16h$) than closer ($x = -10h$). We explain that phenomenon thanks to the average velocity over the capture area, noted \overline{U} , computed from the wake maps (Fig. 3). Since the wake height is lower at $x = -10h$, $\overline{U}(x = -10h) > \overline{U}(x = -16h)$. Hence having $\overline{Cp}(x = -10h) > \overline{Cp}(x = -16h)$ and $\overline{Cx}(x = -10h) > \overline{Cx}(x = -16h)$ is consistent.

Next, $\sigma(Cp)$ is greater behind C1C6 than in Flat floor. At the optimum point it is multiplied by 2.8 at $x = -10h$ and by 1.9 at $x = -16h$. Unlike for the mean values, the effect of the downstream distance on the standard deviation is the same as behind C6 : the fluctuations are greater at $x = -10h$ than at $x = -16h$. Indeed, the close wake is more turbulent than further downstream as previously shown with Fig. 4 where $\tau_{uw}(x = -10h) > \tau_{uw}(x = -16h)$, leading thus to $\sigma(Cp(x = -10h)) > \sigma(Cp(x = -16h))$. The drag's standard deviation is also greater behind C1C6 than in the Flat floor case (multiplied by 1.2 at $x = -10h$ and by 1.3 at $x = -16h$) but to a lesser extent compared to what it is behind C6. On a global point of view, C1C6 seems less impactful than C6 on the turbine behaviour. The key finding here is that the bathymetry must be taken into account when choosing the position of the reference upstream velocity measurement to deduce reliable performance results. To give a closer look at what happens structurally to the turbine, the next sections focus on the best performance operating point for each configuration.

III – 2 Load temporal analysis

Fig. 7 presents a few examples of temporal signals in Flat floor and C6 configurations : the torque applied on the red column (Fig. 1) and two forces measured by the load cell located between the turbine and the base. The massive increase of the fluctuations, observed in the previous section, is also noticeable here, for the torque and for the loads. The other forces and moments, as well as the C1C6 configuration, show the same behaviour, which is summarised in Tab. 1 and 2. Both tables show the impact induced by bathymetry variation on the fluctuations, represented by the standard deviation, and on the extreme values of the loads. Those quantities are of high interest for turbine makers when considering the structural design of their devices.

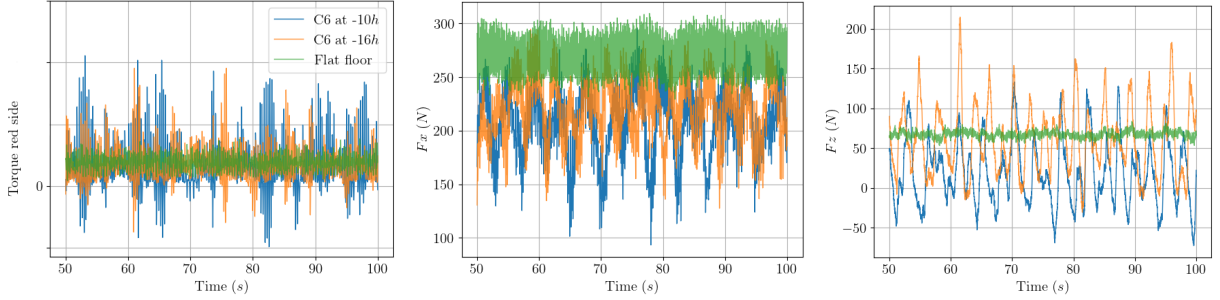


FIGURE 7 – Temporal evolution of Q (left), F_x (middle) and F_z (right) at the best performance point. F_x and F_z come from the load cell located between the turbine and the base.

Between Flat floor and C6 configurations, the fluctuations of the forces rise in every direction and in the same proportion at $x = -10h$ and $x = -16h$. Indeed, the standard deviation is multiplied by approximately 1.7 for F_x , 3.1 for F_y and 10 for F_z . The massive increase of fluctuations in z is clearly visible in Fig. 7 and can be explained by the vertical velocity component brought by the vortices and their rising trajectory behind C6 [9]. The extreme values are much more widely spread behind the obstacle as the range is multiplied by more than 2 for F_x , around 4 for F_y and 7 for F_z , from Flat floor to C6. Those range increases are likely to have a great impact on the structural fatigue. F_x is usually monitored closely for turbines with gravity base because of the slippage risk. Here the maximum F_x value in C6 configuration does not exceed the one of Flat floor. Therefore, for the same inflow velocity, the presence of bathymetry variations does not increase the probability of slippage. However, for the two other components, the highest values can rise by up to a factor 2.5 between Flat floor and C6. This must be considered when looking at rupture issues. The load cell placed under the base shows mainly the same behaviour as the one between the base and the turbine. Yet, we observe a reduction of standard deviations and extreme ranges between 15 and 25 % for the three force components of all configurations presented in this section (except for F_z in Flat floor). The measurement range of the upper load cell is 1.5 kN while it is 20 kN for the lower one. In comparison, the measured forces do not exceed a few hundreds of newtons and the standard deviations a few tens. Therefore, we can assume the measurement range of the lower load cell to be too wide to measure every single variation, resulting in lower standard deviations.

In the tandem configuration, the global behaviour looks similar to the C6 configuration, with an increase of the standard deviation in comparison with the Flat floor case and extreme values more widely spread. However, the level of fluctuation is quite lower here than behind C6 for F_x and for F_z as their standard deviation is divided by 1.4 and 1.8 respectively from C6 to C1C6. The ranges between extreme values are quite smaller too. Their reduction from C6 to C1C6 stands between 13 and 35 % depending on the component and the distance considered. The wake maps of Section II – 3 show that the Reynolds shear stress (Fig. 4) is lower behind C1C6 than behind C6. Therefore the overall turbulence level must be lower which leads to lower standard deviations and extreme ranges. Moreover, [10] showed that the turbulent structures

shed by the C1C6 configuration are two times smaller than those shed by the isolated cylinder. As a consequence, the impact on the turbine is lower as well, leading to a lower risk of fatigue and failure issues.

TABLE 1 – Forces standard deviation and extreme values at the best performance point. Load cell located between the turbine and the base. All values are in N.

Configuration	$\sigma(Fx)$	Fx range	$\sigma(Fy)$	Fy range	$\sigma(Fz)$	Fz range
Flat floor	17.8	228 / 313	10.2	0 / 58	4.0	50 / 84
C6 at x=-10h	32.1	80 / 300	32.5	-104 / 120	40.8	-73 / 166
C6 at x=-16h	28.9	111 / 303	31.2	-105 / 130	39.6	-32 / 215
C1C6 at x=-10h	20.8	142 / 287	32.4	-74 / 121	21.3	-40 / 121
C1C6 at x=-16h	22.5	126 / 280	28.2	-60 / 122	23.1	-32 / 148

The same analysis can be done for the moments (Tab. 2) for which we observe a global increase of the fluctuations and extreme ranges behind C6 compared to Flat floor. This growth is slightly greater with the cylinder at $x = -16h$ than at $x = -10h$ for Mx but it is the other way around for My and Mz . The quantity of highest interest is My because of the turbine toppling risk. Here, we see that the maximum value in C6 cases is very close to the maximum in the Flat floor configuration. Hence, the turbine is unlikely to tip over due to bathymetric obstacles. However, with C6 upstream, Mx and Mz maxima rise by a factor between 2.6 and 5.1 depending on the moment and the distance, possibly leading to failure issues. The load cell located below the foundation shows the same influence of the bathymetry, but with higher values of σ and ranges for Mx and My for all cases. The average value of My is also always much greater (around 2.3 times) but that comes from a greater distance between the load cell and the application point of the force, assuming Fx to be the only force responsible for My . Indeed, previous measurements showed that half of the drag is due to the friction between the structure and the flow while the other half comes from the energy extraction by the rotors' rotation. Thus, the base has an influence only on the friction part and as it is in the boundary layer of the flow it only adds little friction. In Flat floor, \overline{Fx} rises by only 6 % between the upper and the lower load cell. Therefore, we can consider its point of application to be almost at the same location whether we consider the full machine or only the turbine part (excluding the base). We estimate that point of application to be located around the middle of the turbine, that is to say around 23 cm above the upper load cell. 26 cm separate the two load cells, therefore the distance between the point of application of the force and the sensor is more than doubled when we consider the lower load cell and so is the moment My . This explains the increase of My between the two load cells.

In the same way as for the forces, we notice a smaller impact of C1C6 on the moments, particularly for My and Mz . Compared to C6, their standard deviations are divided respectively by 1.3 and 1.4 and their ranges reduction is between 10 and 26 % depending on the component and the distance with the obstacles. The load analysis corroborates what is found in Section III – 1 : a smaller impact when a cube is placed upstream of the cylinder than when the cylinder is isolated.

TABLE 2 – Moments standard deviation and extreme values at the best performance point. Load cell located between the turbine and the base. All values are in Nm.

Configuration	$\sigma(Mx)$	Mx range	$\sigma(My)$	My range	$\sigma(Mz)$	Mz range
Flat floor	6.9	-18 / 23	5.3	39 / 64	2.6	-13 / 8
C6 at x=-10h	14.2	-47 / 48	6.9	13 / 63	9.3	-33 / 41
C6 at x=-16h	16.6	-62 / 61	5.8	18 / 65	7.4	-31 / 33
C1C6 at x=-10h	17.4	-43 / 49	5.9	24 / 69	5.9	-25 / 30
C1C6 at x=-16h	13.2	-37 / 46	5.0	24 / 59	6.4	-32 / 22

III – 3 Load spectral analysis

Fig. 8 presents the Fourier Transform of the torque on the red column and of Fx (load cell between the turbine and the base) for a large frequency range, between 0.1 and 10 Hz . It allows us to look at turbine related phenomena so frequencies are normalised by the rotation frequency (f_r). The other efforts behave the same way as Fx . Only the Flat floor and C6 configurations are displayed here but C1C6 exhibits the same features as C6.

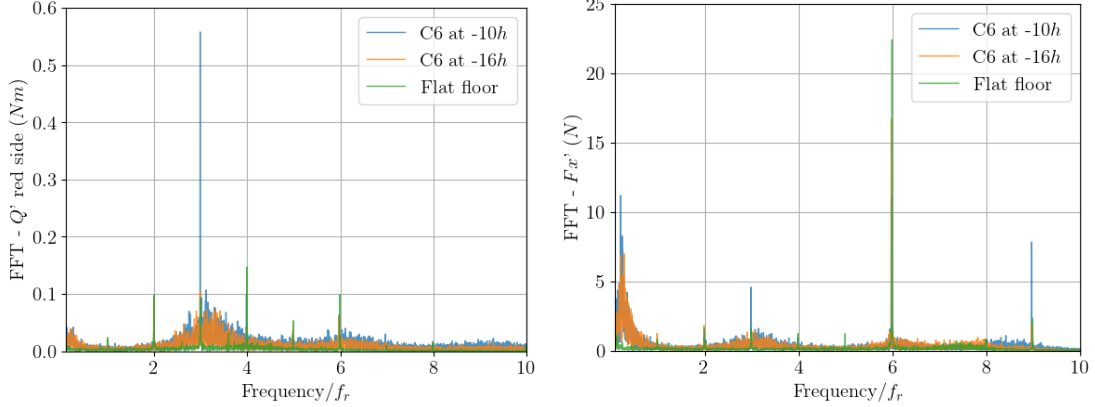


FIGURE 8 – Fourier Transform of Q (left) and Fx (right) in FC at the best performance point, normalised by the rotation frequency.

First of all, looking at the Flat floor configuration, we notice sharp peaks at the harmonics of the rotation frequency. The torque is measured on one column, made of six blades. $6 * f_r$ is therefore the blades passing frequency and we expected to find an important peak there. The peak at $3 * f_r$ may reveal an asymmetry in the torque distribution between the top and bottom rotors while the other harmonics may come from the control system, geometry imperfections or flow asymmetry for instance. In almost the whole frequency range, the behaviour is the same behind the obstacle than in the Flat floor case. The peaks are more widely spread though, the rotors' rotation being disturbed by the turbulence, which results in larger torque and rotational speed ranges as shown by the scatter plots in Fig. 5. Fig. 9 zooms in on low frequencies, between 0.1 and 1 Hz . It compares Flat floor with C6 on one side and with C1C6 on the other one. Fourier Transform of the torque on the red column and of Fx (load cell between the turbine and the base) are displayed. The Flat floor curves present no noticeable event whereas C6 and C1C6 cases have a strong frequency content. This time, the frequencies are not normalised by f_r as we are looking at a flow related phenomenon. For most of the load components, the strongest peaks are between 0.2 and 0.3 Hz . This frequency range corresponds to the large eddies detached from the cylinder at a frequency around 0.25 Hz brought to light in [9]. They seem to affect strongly the 2-VATT and might be responsible for structure failures should a turbine stand in their way. Looking in more details, differences appear when we compare C6 and C1C6. Firstly, the Fourier Transform levels are globally lower for C1C6 than for C6. It means that the energy of the large structures is lower in the tandem configuration, due to a lower turbulence level and smaller vortices as explained in Section III – 2. Secondly, in C6 the phenomenon is stronger close to the obstacle ($x = -10h$) than far ($x = -16h$). [9] explains that high aspect ratio bathymetry variation leads to energetic structures flowing downstream and towards the surface. Here the turbine is installed on the floor, therefore when the structures are ascending in the water column they are likely to avoid the turbine placed further downstream. Yet, in C1C6 the structures have a greater impact when the turbine is far from the obstacles ($x = -16h$) than when it is close ($x = -10h$). As shown in [10], a greater distance is needed for turbulent structures to aggregate behind C1C6 than behind C6 and they move horizontally in the wake. This is why the peak around 0.25 Hz is less noticeable at $x = -10h$ than at $x = -16h$.

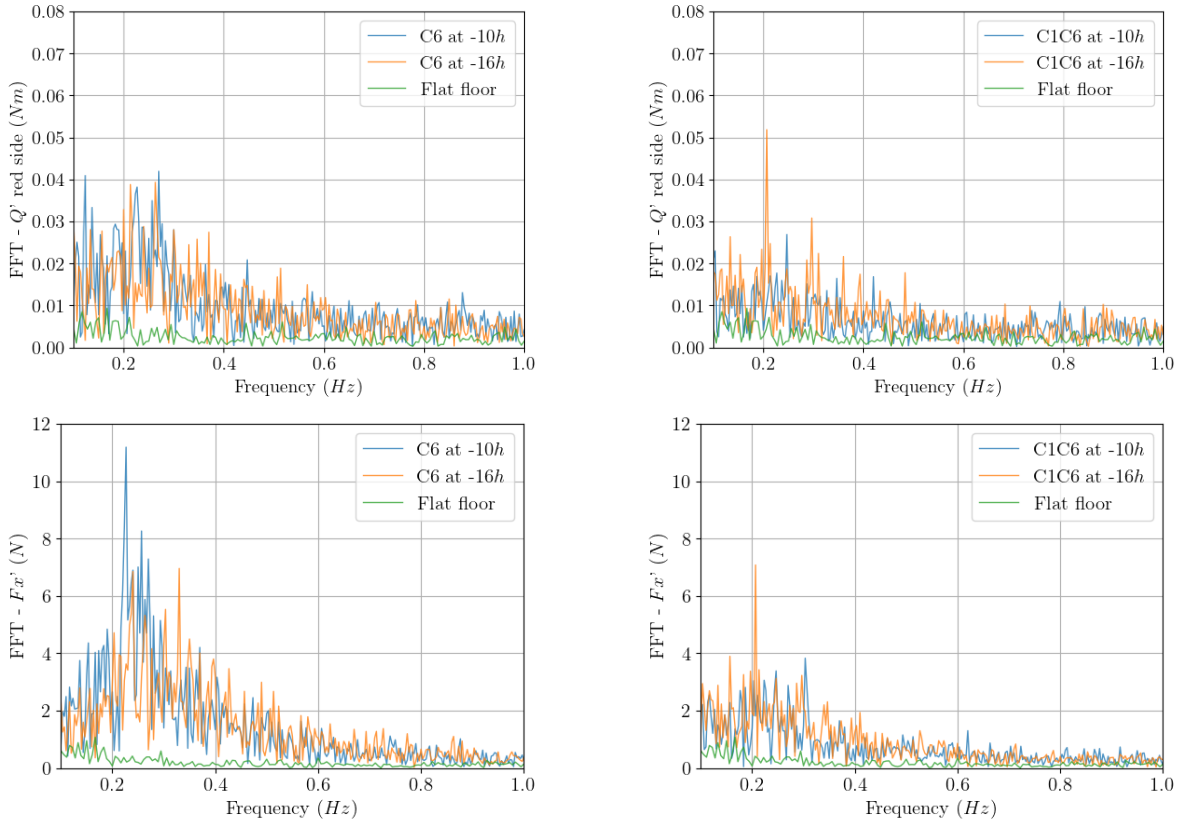


FIGURE 9 – Fourier Transform of Q (top) and Fx (bottom) at the best performance point. Left : C6 ; right : C1C6

IV – Conclusion

This work reports on the response of a ducted twin vertical axis tidal turbine to bathymetry-induced turbulent flows. The experimental study used a bottom-mounted cube and a square cylinder to represent bathymetry variations. Their wakes, analysed in prior works, exhibit an important velocity reduction and large turbulent structures shedding at a frequency around 0.25 Hz. Those energetic vortices flow towards the surface in the wake of the large aspect ratio obstacle while they remain close to the floor in the tandem configuration. Consequently, the mean turbine’s performance and loads are reduced compared to a smooth ocean floor, whereas their fluctuations and extreme ranges substantially increase. The mean values of the power and drag coefficients drop respectively by up to 41 % and 25 % while their standard deviations are multiplied respectively by up to 2.8 and 1.8. The configuration of the obstacles and their distance from the turbine play an important role in its behaviour. When the turbine is close to the bathymetry variation, a large aspect ratio obstacle has a greater impact than the same obstacle with a cube just ahead of it, because the former produces larger and more energetic vortices than the latter. Yet, when the turbine is placed further downstream, the tandem configuration becomes more impacting as its wake develops horizontally rather than rising towards the free surface. That comparison of two kinds of simplified bathymetries shows the complexity of the interaction between bathymetry variation and turbine behaviour. It is therefore necessary to consider each bathymetry specifically when choosing installation sites, for energetic performance assesment as much as for structural design.

Laser Doppler Velocimetry measurements in the turbine’s induction zone will be used to better understand the impact of the obstacles wake on the turbine. On a reverse point of view, they could also help understand how the presence of the turbine modifies the obstacles wake, an interesting question when thinking about future arrays of tidal energy converters.

Références

- [1] A. S. Bahaj, A. F. Molland, J. R. Chaplin, and W. M. Batten. Power and thrust measurements of marine current turbines under various hydrodynamic flow conditions in a cavitation tunnel and a towing tank. *Renewable Energy*, 32(3) :407–426, 2007.
- [2] T. Blackmore, L. E. Myers, and A. S. Bahaj. Effects of turbulence on tidal turbines : Implications to performance, blade loads, and condition monitoring. *IJME*, 2016.
- [3] L. Furgerot and al. One year of measurements in Alderney Race : preliminary results from database analysis. *Philosophical Transactions of the Royal Society A*, 378, 2020.
- [4] B. Gaurier and al. MaRINET2 tidal energy round robin tests-performance comparison of a horizontal axis turbine subjected to combined wave and current conditions. *Journal of Marine Science and Engineering*, 8(6), 2020.
- [5] B. Gaurier, M. Ikhennicheu, G. Germain, and P. Druault. Experimental study of bathymetry generated turbulence on tidal turbine behaviour. *Renewable Energy*, 156 :1158–1170, 2020.
- [6] N. Guillou, S. P. Neill, and J. Thiébot. Spatio-temporal variability of tidal-stream energy in north-western Europe. *Phil. Trans. R. Soc. A*, 378(2178) :20190493, 2020.
- [7] M. Harrold and P. Ouro. Rotor loading characteristics of a full-scale tidal turbine. *Energies*, 12(6), 2019.
- [8] M. Ikhennicheu, G. Germain, P. Druault, and B. Gaurier. Experimental investigation of the turbulent wake past real seabed elements for velocity variations characterization in the water column. *International Journal of Heat and Fluid Flow*, 78(June) :108426, 2019.
- [9] M. Ikhennicheu, G. Germain, P. Druault, and B. Gaurier. Experimental study of coherent flow structures past a wall-mounted square cylinder. *Ocean Engineering*, 2019.
- [10] M. Magnier, P. Druault, B. Gaurier, and G. Germain. Comparison of bathymetry variation effects on tidal turbine behaviour. In *Journées de l'hydrodynamique*, pages 1–12, 2020.
- [11] M. Magnier, P. Druault, and G. Germain. Experimental investigation of upstream cube effects on the wake of a wall-mounted cylinder : Wake rising reduction, TKE budget and flow organization. *European Journal of Mechanics, B/Fluids*, 87 :92–102, 2021.
- [12] M. Moreau, G. Germain, G. Maurice, and A. Richard. Sea states influence on the behaviour of a bottom mounted full-scale twin vertical axis tidal turbine. *Ocean Engineering*, 2022.
- [13] M. Moreau, G. Maurice, J. V. Facq, and G. Germain. Experimental study of two opposed flow directions effect on a ducted twin vertical axis tidal turbine. In *RENEW*, 2022.
- [14] R. Murray. *Passively adaptive tidal turbine blades : Design methodology and experimental testing*. PhD thesis, Dalhousie University, 2016.
- [15] P. Mycek, B. Gaurier, G. Germain, G. Pinon, and E. Rivoalen. Experimental study of the turbulence intensity effects on marine current turbines behaviour. Part I : One single turbine. *Renewable Energy*, 66 :729–746, 2014.